Precision tracking control by pneumatic actuator: challenges for input delay and acoustic vibrations

Wataru Ohnishi[*a)] Member, Hiroshi Fujimoto[*] Senior Member

A pneumatic actuator has several advantages such as low heat generation, a high power-to-weight ratio, and low costs; however, it also has disadvantages such as time delays, nonlinearities, and position-dependent multiple pressure resonances. Essentially, the delay in the pneumatic control loop is not negligible because the speed of sound is about one million times slower than the speed of light. The delay degrades the bandwidth of the feedback control, due to its nonminimum phase characteristics. Additionally, the slow speed of the compressional wave causes the chamber length dependent vibrations. This paper briefly introduces studies about these challenges.

Keywords: Pneumatic actuator, time delay compensation, vibration suppression

1. Introduction

High precision stages are an important type of device used in semiconductor and flat panel display manufacturing processes [(1)(2)]. In order to achieve high integration and to reduce the manufacturing cost of electronic devices, more precise and more accurate positioning using larger stages is required [(3)(4)]. In order to satisfy these two requirements, a dual-stage structure having a short stroke fine stage and a long stroke coarse stage is commonly used [(1)]. Although linear motors and ball screws are normally used in coarse stages, the electric motor becomes heavier and heat generation increases due to high acceleration and large stage requirements [(5)]. Variations in temperature have severe effects on the measurement system and lens apparatus [(6)(7)], and thus precise temperature control [(7)] is problematic.

The motivation of our study is to replace the linear motor/ball screw implemented in the coarse stage with a pneumatic actuator. A pneumatic actuator has the following advantages compared with a linear motor: 1) low heat generation [(6)]; 2) high power-to-weight ratio [(8)(9)]; and 3) low cost [(8)]; but its disadvantages also include: 1) a time delay [(10)]; 2) nonlinear dynamics [(9)(11)~(14)] due to air dynamics and servo valves; and 3) position-dependent resonances [(15)]. These properties limit the bandwidth of the pressure feedback bandwidth. A common structure for positioning control has a pressure feedback control as an inner loop and a position feedback as an outer loop. Because pressure is proportional to the force applied to the stage, a pressure feedback control is no less important than the current control for linear motor drive. This paper briefly summarizes the recent results of the input delay compensation and resonance cancellation method by the authors.

To address the time delay problem, we have proposed a modified Smith predictor and applied it to a pneumatically actuated scan stage to achieve high-bandwidth pressure feedback [(16)]. Since the standard Smith predictor is not applicable to the system with a pure integrator, we implemented an additional high-pass filter to cancel the integration. The proposed high-bandwidth controller effectively suppresses the friction disturbance, especially at the velocity reversal.

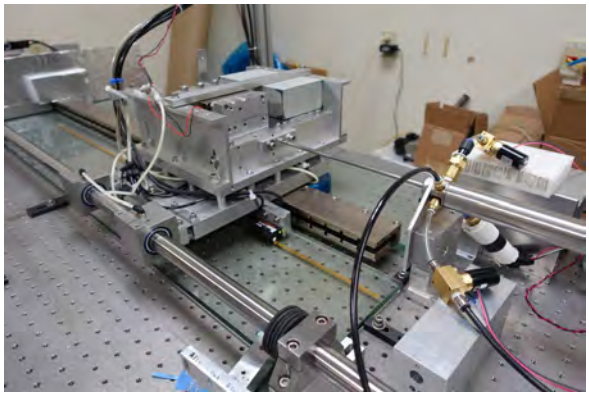

Fig. 1. Photograph of the pneumatic actuated scan stage [(16)].

In addition to the delay, the position-dependent resonances limit the pressure feedback bandwidth [(15)]. The resonances are functions of the chamber length, valve position, and pressure sensor position. Moreover, the resonances have multiple modes with a high peak in the frequency domain. To address the problem, we have proposed a modeling and vibration cancellation method for a pneumatic cylinder based on acoustic wave equation [(15)]. This model fits the frequency response with multiple resonances based on delay elements, taking into account the damping effect of the system. Using the wave equation based model, we have proposed a wave cancellation filter to cancel multiple modes and shape it as a single integrator. The filter comprises delay elements and a first-order filter.

2. Input delay compensation by modified Smith predictor [(16)]

Photograph and schematic of a pneumatic actuated scan

a) Correspondence to: ohnishi@koseki.t.u-tokyo.ac.jp
* The University of Tokyo
7-3-1 Hongo, Bunkyo-ku, Tokyo, 113-8656, Japan

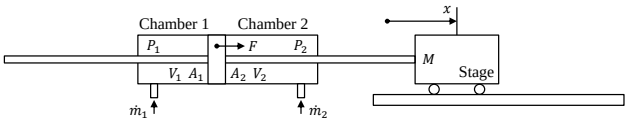

Fig. 2. Model of the pneumatic actuated scan stage [16].

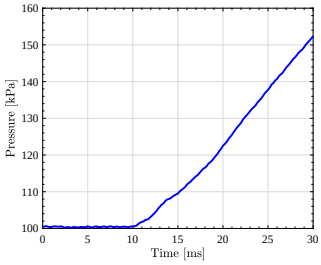

Fig. 3. Input delay of the pneumatic chamber. Voltage step input is applied to a valve at $t = 0$ and about 10 ms delay is observed [16].

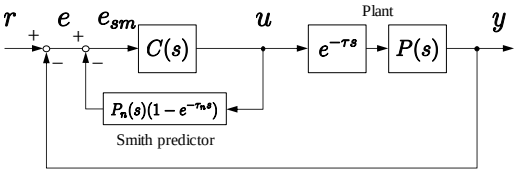

Fig. 4. Block diagram of the Smith predictor [16].

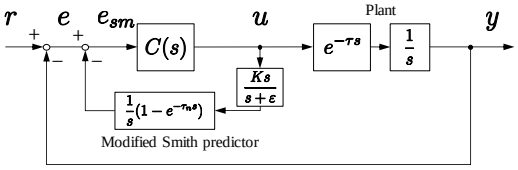

Fig. 5. Block diagram of the modified Smith predictor [16].

stage are shown in Fig. 1 and Fig. 2. Generally, a cylinder is composed of two chambers. The product of the cross-sectional area and the pressure difference of the two chambers is applied to the stage as a force. Therefore, precise pressure control is a key for precision positioning control.

However, Fig. 3 shows that there is input delay from the valve current to the chamber pressure variation. It may degrade the pressure control bandwidth because of its non-minimum phase characteristics [17]. Actually, delay in the pneumatic control loop is inevitable because the speed of sound is about one million times slower than the speed of light.

2.1 Modified Smith predictor Various methods have been studied to address time delay: 1) Smith predictor [18] and its modifications [19][20], 2) Internal Model Control (IMC) [21], and 3) communication disturbance observer [22].

Since the considered control object has an integrator [16], the standard Smith predictor is not applicable [20]. We have proposed a modified Smith predictor [16] to a trajectory tracking control problem for a plant with an integrator. Unlike the standard Smith predictor shown in Fig. 4, the proposed modified Smith predictor shown in Fig. 5 has a high-pass filter and an extra gain K as tuning parameters. The high-pass filter enables us to avoid the integration under a constant disturbance (e.g. gravitational force).

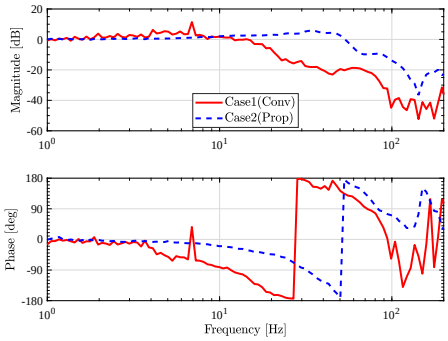

Fig. 6. Pressure feedback control performance $\frac{\hat{f}(j\omega)}{f^{ref}(j\omega)}$. By applying the modified Smith predictor, the feedback bandwidth is improved as listed in Table 1 [16].

Table 1. Pressure feedback control performance by Fig. 6 [16].

	Case1 (Conv)	Case2 (Prop)
Pressure FB	low gain	high gain + MSP*
Gain margin	13dB (32Hz)	6.4dB (62Hz)
Phase margin	35deg (6.9Hz)	35deg (27Hz)
Bandwidth	9.4Hz	31Hz

*Modified Smith predictor

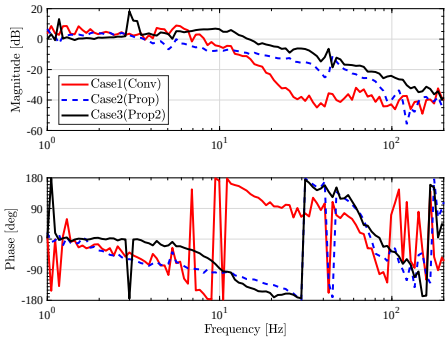

Fig. 7. Position control performance $\frac{x(j\omega)}{x^{ref}(j\omega)}$. Position feedback bandwidth is improved as listed in Table 2 [16].

Table 2. Position feedback control performance by Fig. 7 [16].

	Case1 (Conv)	Case2 (Prop)	Case3 (Prop2)
Pressure FB	low gain	high gain + MSP*	same as Case 2
Position FB	low gain	same as Case 1	high gain
Gain margin (Position FB)	7.0 dB (9 Hz)	17 dB (30 Hz)	9.6 dB (30 Hz)
Phase margin (Position FB)	22 deg (5.9 Hz)	53 deg (3.2 Hz)	26 deg (10 Hz)
Bandwidth (Position FB)	5.3 Hz	7.7 Hz	11 Hz

*Modified Smith predictor

Table 3. Scan motion experimental results by Fig. 8 [16].

	Case1 (Conv)	Case2 (Prop)	Case3 (Prop2)
Maximum tracking error	508 μm	418 μm	135 μm
Standard deviation of the tracking error	114 μm	94.0 μm	19.5 μm

2.2 Feedback bandwidth improvement by modified Smith predictor Performance of the pressure feedback control, which is an inner loop feedback control, is shown in Fig. 6 and Table 1. By keeping the same phase margin, Case

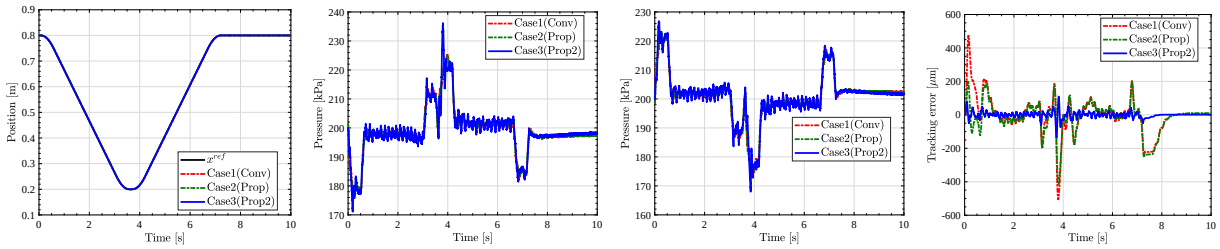

(a) Stage position x_m. (b) Chamber 1 pressure P_1. (c) Chamber 2 pressure P_2. (d) Stage position tracking error.

Fig. 8. Scan motion experimental results [16]. The tracking error is drastically reduced by the proposed method (Case3).

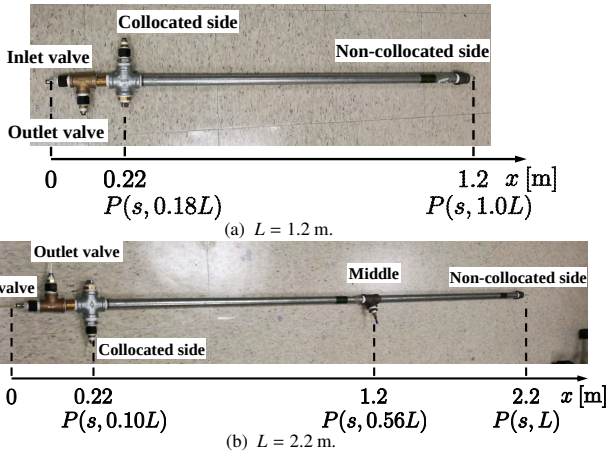

(a) L = 1.2 m.

(b) L = 2.2 m.

Fig. 9. The two lengths chambers [15].

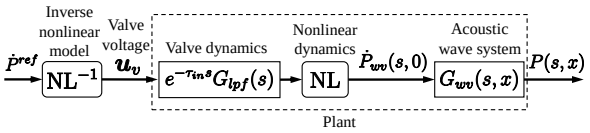

Fig. 10. Plant model for a single chamber [15].

Table 4. List of symbols [15]

Symbols	Definition	Value	Unit
ρ	density		kg/m^3
p	pressure		Pa
v	flow speed		m/s
γ	heat capacity ratio	1.402	-
c_0	speed of sound		m/s
R	ideal gas constant	287.1	J/(kg · K)
T	temperature (Kelvin)		K
x	pressure sensor position		m

2 can increase the gain and have higher pressure feedback bandwidth.

Performance of the position feedback control, which is an outer loop feedback control, is shown in Fig. 7 and Table 2.

2.3 Scan motion experiment Scan motion experiment is performed with the modified Smith predictor as shown in Fig. 8. The stage motion trajectory is shown in Fig. 8(a). Fig. 8(d) shows that the tracking error is drastically reduced by Case 3, especially the moment of the velocity reversal.

3. Acoustic wave cancellation by damping considered wave equation [15]

In addition to the input delay, pneumatic actuators has position dependent resonances. Essentially, this is caused by the slow compressional wave and its internal delay of the system.

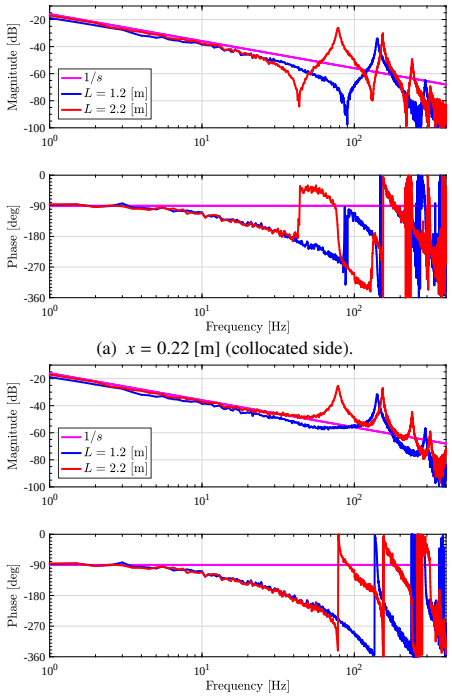

(a) x = 0.22 [m] (collocated side).

(b) $x = 1.0L$ (non-collocated side).

Fig. 11. Chamber length dependency of $\frac{P(s,x)}{\dot{P}^{ref}(s)}$ [15].

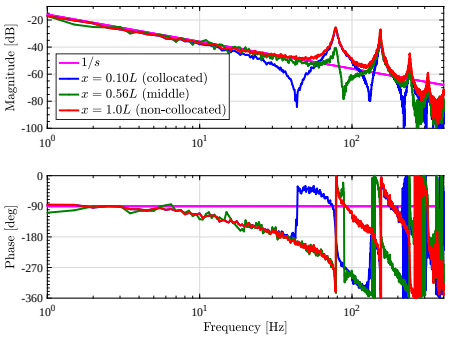

Fig. 12. Sensor position dependency of $\frac{P(s,x)}{\dot{P}^{ref}(s)}$, ($L$ = 2.2m) [15].

3.1 Modeling

3.1.1 Experimental setup The experimental setups of the resonance modeling are shown in Fig. 9. This chamber had inlet and outlet poppet vales on one end. The inlet valve was connected to a high-pressure source (400 kPa) and the outlet valve was connected to the ambient air. Pressure

sensors were implemented on the valve side, the other side of the chamber, and the middle of the chamber. Two chambers with different lengths were prepared to investigate the chamber length and sensor position dependency.

3.1.2 Chamber length dependency Plant model for single chamber is shown in Fig. 10. NL denotes nonlinear dynamics of the valve and air flow equation [6][23][24]. To compensate the nonlinearity by nonlinear inversion, the relationship between the inlet and outlet valve voltages ($\boldsymbol{u}_v$), mass flow rate, and chamber pressure is modeled by a polynomial [12]. Dead-zone compensation is also used for the valve nonlinearity between the valve voltages ($\boldsymbol{u}_v$) and size of orifice areas. The frequency responses of the systems in Fig. 9 are shown in Figs. 11 and 12 which both illustrate the chamber length dependency and sensor position dependency, respectively.

3.1.3 Wave equation [25] The variables are listed in Table 4. A one-dimensional wave, constant cross-sectional area, isentropic change, and non-static flow are assumed. According to equation of continuity, Euler's equation of motion, equation of isentropic change, and ideal gas low, the following wave equations are obtained. For detail, refer to [25].

$$\frac{\partial^2 p}{\partial t^2} - c_0^2 \frac{\partial^2 p}{\partial x^2} = 0 \cdots\cdots (1)$$

3.1.4 Transfer function The boundary conditions are given by (2) by considering a fixed end condition [26] and a dimensional analysis,

$$c_o^2 \frac{\partial p(t,x)}{\partial x}\bigg|_{x=0} = -u(t), \quad \frac{\partial p(t,x)}{\partial x}\bigg|_{x=L} = 0, \cdots\cdots (2)$$

where the control input $u(t)$ is $L\frac{\partial^2 p_{ww}(t,0)}{\partial t^2}$. $p_{wv}(t,0)$ denotes the pressure wave created by the inlet and outlet valves located at $x = 0$. The Laplace transform of (1) is

$$a^2 s^2 P(s,x) = \frac{\partial^2 P(s,x)}{\partial x^2}, \cdots\cdots (3)$$

where a denotes $\frac{1}{c_0}$. From (2) and (3), we obtain

$$\frac{\partial P(s,0)}{\partial x} = -a^2 U(s), \quad \frac{\partial P(s,L)}{\partial x} = 0. \cdots\cdots (4)$$

The general solution is given by

$$P(s,x) = C_1 \cosh(axs) + C_2 \sinh(axs). \cdots\cdots (5)$$

By partial differentiation of (5) with respect to x, the following equation is obtained.

$$\frac{\partial P(s,x)}{\partial x} = C_1 sa \sinh(axs) + C_2 sa \cosh(axs) \cdots\cdots (6)$$

According to (4) and (6), integral constants are obtained by

$$C_1 = \frac{a}{s}\frac{\cosh(aLs)}{\sinh(aLs)} U(s), \quad C_2 = -\frac{a}{s} U(s). \cdots\cdots (7)$$

The transfer function from $U(s)$ to $P(s,x)$ is

$$\begin{aligned}\frac{P(s,x)}{U(s)} &= \frac{a}{s}\frac{\cosh(aLs)}{\sinh(aLs)}\cosh(axs) - \frac{a}{s}\sinh(axs) \\ &= \frac{a}{s}\frac{\cosh(aLs)\cosh(axs) - \sinh(aLs)\sinh(axs)}{\sinh(aLs)} \\ &= \frac{a}{s}\frac{\cosh[as(L-x)]}{\sinh(aLs)}. \cdots\cdots (8)\end{aligned}$$

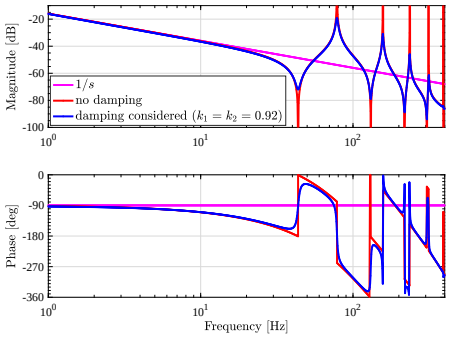

Fig. 13. Effect of damping ($x = 0.10L$) [15].

Table 5. Parameters for fitting and wave cancellation filter design [15].

Symbols	Definition	Value	Unit
c_0	speed of sound	343.4	m/s
L	chamber length	2.2	m
k_1, k_2	damping coefficient	0.92, 0.92	-
τ_{in}	input delay	1.8	ms
ζ_1, ζ_2	damping coefficient of the valve dynamics	0.70, 0.70	-
ω_1, ω_2	cutoff frequency of the valve dynamics	90, 170	Hz

From the above, the acoustic wave system is derived.

$$\frac{P(s,x)}{\dot{P}_{wv}(s)} = \frac{L}{c_0}\frac{e^{-\frac{x}{c_0}s} + e^{-\frac{2L-x}{c_0}s}}{1 - e^{-\frac{2L}{c_0}s}}. \cdots\cdots (9)$$

According to (9), the transfer functions from the valve input to the valve side end ($x = 0$) pressure and the other side end ($x = L$) pressure are given as

$$\frac{P(s,0)}{\dot{P}_{wv}(s)} = \frac{L}{c_0}\frac{1 + e^{-\frac{2Ls}{c_0}}}{1 - e^{-\frac{2Ls}{c_0}}}, \cdots\cdots (10)$$

$$\frac{P(s,L)}{\dot{P}_{wv}(s)} = \frac{L}{c_0}\frac{2e^{-\frac{Ls}{c_0}}}{1 - e^{-\frac{2Ls}{c_0}}}. \cdots\cdots (11)$$

3.1.5 Modified acoustic wave equation considering damping The model defined in (9) does not take into account the damping, so the gain becomes 0 at anti-resonances and $+\infty$ at resonances. However, the measured frequency responses shown in Figs. 11 and 12 indicate that the system experiences damping. Thus, damping coefficients $0 < k_1 < 1$, $0 < k_2 < 1$ are introduced to model this phenomenon.

$$\begin{aligned}G_{wv}(s,x) &= \frac{P(s,x)}{\dot{P}_{wv}(s)} \\ &= \frac{2L}{c_0}\frac{k_1}{1+k_2}\frac{s + \frac{1-k_1}{k_1}\frac{c_0}{2L}}{s}\frac{e^{-\frac{xs}{c_0}}(1 + k_2 e^{-\frac{2(L-x)s}{c_0}})}{1 - k_1 e^{-\frac{2Ls}{c_0}}} \quad (12)\end{aligned}$$

The coefficients are determined to be a single integrator in a low frequency range, considering that the measured frequency response shown in Figs. 11 and 12 well matches a single integrator blow 3 Hz. Note that

$$\lim_{s\to 0} sG_{wv}(s,x) = 1. \cdots\cdots (13)$$

The effect of damping is shown in Fig. 13. From (12), the valve side end ($x = 0$) and the other side end ($x = L$) transfer functions are modeled by

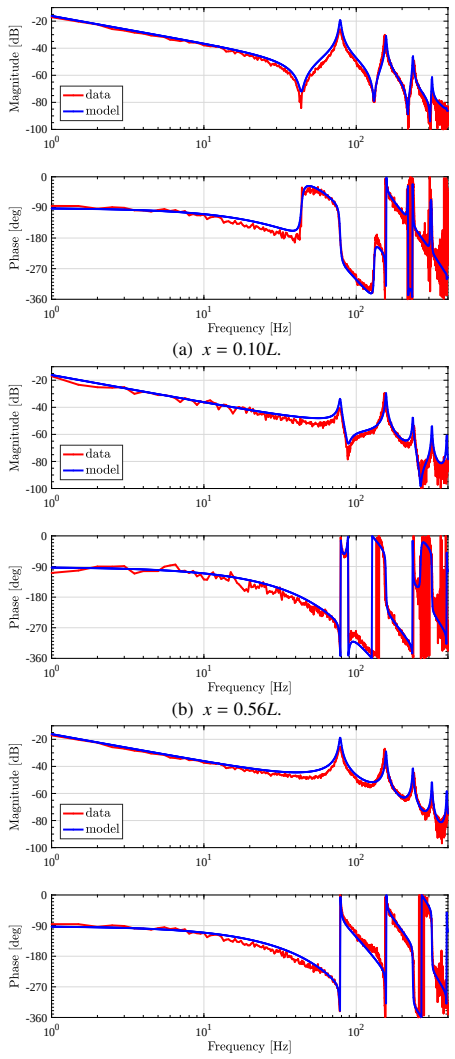

(a) $x = 0.10L$.

(b) $x = 0.56L$.

(c) $x = 1.0L$.

Fig. 14. Fitted by (17) and Table 5 [15].

$$G_{wv}(s,0) = \frac{P(s,0)}{\dot{P}_{wv}(s)} = \frac{2L}{c_0}\frac{k_1}{1+k_2}\frac{s+\frac{1-k_1}{k_1}\frac{c_0}{2L}}{s}\frac{1+k_2e^{-\frac{2Ls}{c_0}}}{1-k_1e^{-\frac{2Ls}{c_0}}} \quad (14)$$

$$G_{wv}(s,L) = \frac{P(s,L)}{\dot{P}_{wv}(s)} = \frac{2L}{c_0}\frac{k_1}{1+k_2}\frac{s+\frac{1-k_1}{k_1}\frac{c_0}{2L}}{s}\frac{e^{-\frac{Ls}{c_0}}(1+k_2)}{1-k_1e^{-\frac{2Ls}{c_0}}}. \quad (15)$$

3.1.6 Valve model Poppet valves are used in this setup. The valve dynamics are modeled by a fourth order low pass filter and input delay

$$G_{lpf}(s)e^{-\tau_{in}s} = \frac{\omega_1^2}{s^2+2\zeta_1\omega_1 s+\omega_1^2}\frac{\omega_2^2}{s^2+2\zeta_2\omega_2 s+\omega_2^2}e^{-\tau_{in}s} \quad (16)$$

Considering the valve dynamics, the transfer function from $\dot{P}^{ref}(s)$ to pressure $P(s,x)$ in Fig. 10 is obtained assuming perfect nonlinearity compensation.

$$\frac{P(s,x)}{\dot{P}^{ref}(s)} = G_{wv}(s,x)G_{lpf}(s)e^{-\tau_{in}s} \quad (17)$$

The fitting results by (17) and parameters in Table 5 are shown in Fig. 14. The position-dependent multiple resonances are modeled well by the single equation.

3.2 Wave cancellation filter

3.2.1 Case ignoring damping Figs. 11, 12, and (10) indicate that the plant model have an integrator in a low frequency range. To cancel the all resonances and anti-resonances, the integrator and the rest are separated as follows

$$\frac{P(s,0)}{\dot{P}^{ref}(s)} = \frac{1}{s}\frac{Ls(1+e^{-\frac{2Ls}{c_0}})}{c_0(1-e^{-\frac{2Ls}{c_0}})} \quad (18)$$

The wave cancellation filter C_{wcf} for $(x = 0)$ is obtained by inversion of the resonant modes as follows

$$C_{wcf}(s,0) = \frac{c_0(1-e^{-\frac{2Ls}{c_0}})}{Ls(1+e^{-\frac{2Ls}{c_0}})} \quad (19)$$

3.2.2 Case considering damping The generalized wave cancellation filter is obtained using the same procedure employed in subsection 3.2.1 for (12) as follows.

$$C_{wcf}(s,x) = \frac{c_0}{2L}\frac{1+k_2}{k_1}\frac{1}{s+\frac{1-k_1}{k_1}\frac{c_0}{2L}}\frac{1-k_1e^{-\frac{2Ls}{c_0}}}{1+k_2e^{-\frac{2(L-x)s}{c_0}}} \quad (20)$$

3.3 Experiments

A block diagram is shown in Fig. 15. A proportional-integral (PI) and phase-lead controller are used for feedback. The pressure reference is the first-order delayed step. α denotes the pole of the low-pass filter used for trajectory generation. $\frac{1}{s}$ is used as a nominal model of the pressure feedforward controller.

The step response is shown in Fig. 16. The pressure vibration is canceled well with the wave cancellation filter. Fig. 16(c) shows the frequency analysis of Fig. 16(b), where up to the fourth mode is observed without the wave cancellation filter. This demonstrates that the proposed wave cancellation filter attenuates multiple modes with a single filter.

4. Conclusion

Pneumatic actuators have several advantages such as light-weight, low heat generation, and low cost. However, due to its inevitable slow propagation speed of the compressional wave, the pneumatic actuator has several disadvantages such as input delay, position-dependent resonances, and nonlinearities.

This paper briefly summarized the recent results of the input delay compensation and resonance cancellation. By applying the modified Smith predictor, the pressure bandwidth is improved and better tracking performance is obtained. However, the position-dependent resonance arises and further bandwidth improvement becomes difficult.

Inherently, there is the infinite number of resonances because the system is described by the wave equation. By applying the wave cancellation filter with damping factor consideration, the precise pressure tracking performance is achieved.

By applying the advanced motion control technique, the disadvantages of the pneumatic actuator are relaxed. We hope that pneumatic actuators become a new option of the linear drive actuator of high-precision industries which requires light-weight actuators.

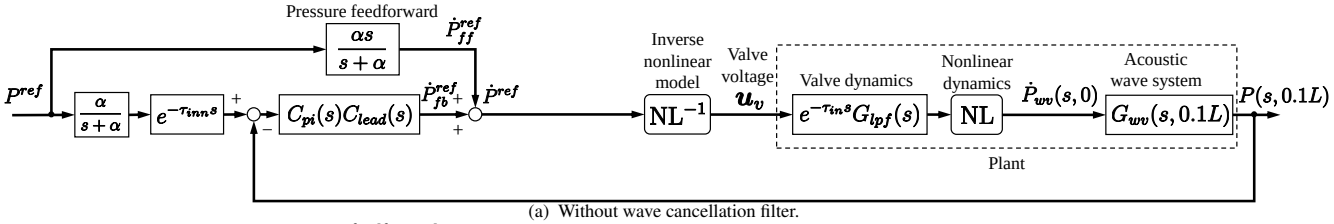

(a) Without wave cancellation filter.

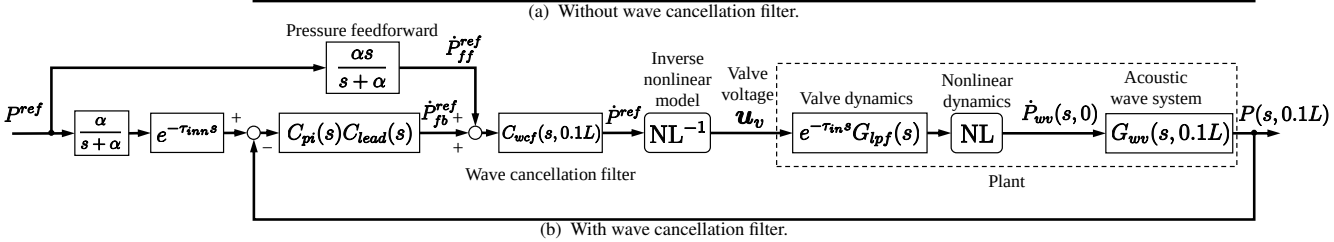

(b) With wave cancellation filter.

Fig. 15. Block diagram with pressure feedforward [15].

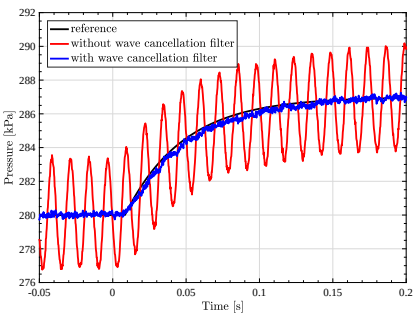

(a) Pressure responses.

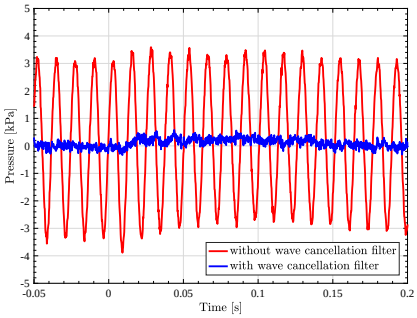

(b) Pressure tracking error.

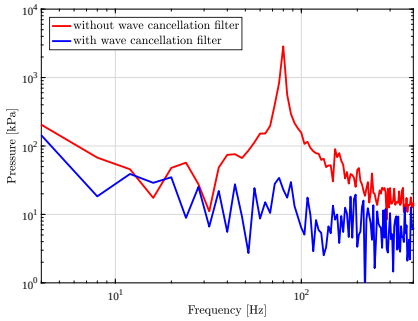

(c) Frequency analysis for (b).

Fig. 16. Step response experiments [15].

References

(1) H. Butler, "Position Control in Lithographic Equipment," *IEEE Control Systems Magazine*, vol. 31, no. 5, pp. 28–47, 2011.

(2) K. Saiki, A. Hara, K. Sakata, and H. Fujimoto, "A Study on High-Speed and High-Precision Tracking Control of Large-Scale Stage Using Perfect Tracking Control Method Based on Multirate Feedforward Control," *IEEE Transactions on Industrial Electronics*, vol. 57, no. 4, pp. 1393–1400, 2010.

(3) M. F. Heertjes, "Variable Gains in Motion Control of Wafer Scanners," *IEEJ Journal of Industry Applications*, vol. 5, no. 2, pp. 90–100, 2016.

(4) T. Oomen, "Advanced Motion Control for Precision Mechatronics: Control, Identification, and Learning of Complex Systems," *IEEJ Journal of Industry Applications*, vol. 7, no. 2, pp. 127–140, 2018.

(5) T. Goto and M. Yuasa, "Recent Control Technology for Semiconductor Exposure Appratus," *Journal of the Society of Instrument and Control Engineers*, vol. 52, no. 5, pp. 425–429, 2013. (in Japanese)

(6) T. Kagawa, K. Sakaki, L. R. Tokashiki, and T. Fujita, "Accurate Positioning of a Pneumatic Servo System With Air Bearings," in *Proceedings of the JFPS International Symposium on Fluid Power*, pp. 693–698, 2002.

(7) Y. Shibazaki, H. Kohno, and M. Hamatani, "An innovative platform for high-throughput, high-accuracy lithography using a single wafer stage," in *Proc. SPIE 7274*, pp. 1–12, 2009.

(8) I. Ramírez, "Modeling and tracking control of a pneumatic servo positioning system," in *2nd International Congress of Engineering Mechatronics and Automation*, pp. 1–6, 2013.

(9) A. Poon, R. Mai, Y. Choi, S. Lee, P.-H. Yang, G. Keswani, A. Hara, and K. Sakata, "Pneumatic Actuator for Precision Motion Control Applications," in *The 10th JFPS International Symposium on Fluid Power*, 2017.

(10) Y. Nakamura, H. Kawakami, and S. Wakui, "Suppression of Anti-Resonance and Resonance in Pneumatic System of Vibration Isolator Considering Time Delay," in *41st Annual Conference of the IEEE Industrial Electronics Society*, pp. 2509–2514, 2015.

(11) E. Richer and Y. Hurmuzlu, "A High Performance Pneumatic Force Actuator System Part 1 - Nonlinear Mathematical Model," *ASME Journal of Dynamic Systems, Measurement, and Control*, vol. 122, no. 3, pp. 416–425, 2001.

(12) Z. Rao and G. M. Bone, "Nonlinear modeling and control of servo pneumatic actuators," *IEEE Transactions on Control Systems Technology*, vol. 16, no. 3, pp. 562–569, 2008.

(13) A. C. Valdiero, C. S. Ritter, C. F. Rios, and M. Rafikov, "Nonlinear mathematical modeling in pneumatic servo position applications," *Mathematical Problems in Engineering*, vol. 2011, 2011.

(14) Y. Shirato, W. Ohnishi, and T. Koseki, "Two-Degree-of-Freedom Control with Adaptive Dead Zone Compensation for Pneumatic Valves," in *SAMCON2019*, pp. 1–6, 2019.

(15) W. Ohnishi, H. Fujimoto, P.-H. Yang, P.-W. Chang, B. Yuan, K. Sakata, and A. Hara, "Acoustic Wave Equation Based Modeling and Collocated Side Vibration Cancellation for Pneumatic Cylinder," *IEEJ Journal of Industry Applications*, vol. 7, no. 2, pp. 109–116, 2018.

(16) W. Ohnishi, H. Fujimoto, K. Sakata, A. Hara, and K. Saiki, "Trajectory Tracking Control for Pneumatic Actuated Scan Stage with Time Delay Compensation," in *42nd Annual Conference of IEEE Industrial Electronics Society*, pp. 5125–5130, 2016.

(17) S. Skogestad and I. Postlethwaite, *Multivariable feedback control: analysis and design*. Wiley, 2005.

(18) O. J. M. Smith, "A Controller to Overcome Dead Time," *ISA Journal*, vol. 6, no. 2, pp. 28–33, 1959.

(19) K. Watanabe and M. Ito, "A process-model control for linear systems with delay," *IEEE Transactions on Automatic Control*, vol. 26, no. 6, pp. 1261–1269, 1981.

(20) K. Åström, C. Hang, and B. Lim, "A new Smith predictor for controlling a process with an integrator and long dead-time," *IEEE Transactions on Automatic Control*, vol. 39, no. 2, pp. 343–345, 1994.

(21) M. Morari and E. Zafiriou, *Robust Process Control*. Prentice Hall, 1989.

(22) K. Natori and K. Ohnishi, "A design method of communication disturbance observer for time-delay compensation, taking the dynamic property of network disturbance into account," *IEEE Transactions on Industrial Electronics*, vol. 55, no. 5, pp. 2152–2168, 2008.

(23) A. H. Shapiro, *The Dynamics and Thermodynamics of Compressible Fluid Flow*. John Wiley & Sons, 1953.

(24) R. B. Goodman, *A Primer on Pneumatic Valves and Controls*. Krieger Pub Co, 1997.

(25) K. Matsuo, *Compressible fluid dynamics: theory and analysis in internal flow*. Ohmsha, 2013. (in Japanese)

(26) H. Alli and T. Singh, "On the feedback control of the wave equation," *Journal of Sound and Vibration*, vol. 234, no. 4, pp. 625–640, 2000.